Penetration and Relaxation in Dry Granular Materials: Insights from Photoelasticity

Sichuan Huang, Ph.D., A.M.ASCE¹; Nariman Mahabadi, Ph.D., A.M.ASCE²; and Junliang Tao, Ph.D., A.M.ASCE³

¹Postdoctoral Research Scholar, School of Sustainable Engineering and the Built Environment, Center for Bio-Mediated and Bio-Inspired Geotechnics (CBBG), Arizona State Univ., Tempe, AZ. Email: sichuan.huang@asu.edu

²Assistant Professor, Dept. of Civil Engineering, Univ. of Akron, Akron, OH.

Email: nmahabadi@uakron.edu

³Associate Professor, School of Sustainable Engineering and the Built Environment, Center for Bio-Mediated and Bio-Inspired Geotechnics (CBBG), Arizona State Univ., Tempe, AZ.

Email: julian.tao@asu.edu

ABSTRACT

Penetration is involved in many geotechnical engineering practices such as site characterization and pile installation. In this study, we investigated the influence of pausing-induced stress relaxation on the penetration process using photoelasticity. A thin cone penetrometer was designed and penetrated a photoelastic granular specimen in two different ways: one is continuous penetration, during which the penetrometer penetrates the specimen continuously for a target travel distance; the other is termed as intermittent penetration, which consists of two short penetration stages separated by a long pausing stage. The penetration rate and overall penetrometer travel distance for the two cases are kept the same. Stress relaxation was observed during the pausing stage and the influence of stress relaxation on the subsequent penetration process was evaluated by comparing the penetration resistance, and force chains, stress field, and displacement field of the granular specimen. Results indicate that pausing-induced stress relaxation is due to particle rearrangement and causes reduction in penetration resistance within a limited travel distance.

INTRODUCTION

Soil penetration is ubiquitous in geotechnical engineering activities, such as soil sampling, site soil characterization, pile installation, tunneling etc. The soil penetration resistance and associated energy consumption are closely related to the soil properties. It has been confirmed that time-dependent chemical, microbiological or mechanical processes may exist and cause structural or compositional changes in soil, resulting in time effects of soil properties. Example phenomena include the time-dependent cone penetration resistance found in freshly deposited or densified sands (Charlie et al. 1992), and the increase of bearing capacity of driven or jacked piles after installation (Bowman and Soga 2005; Chow et al. 1997).

Creep and stress relaxation are two common time-dependent behaviors, which are attributed to particle rearrangements and/or particle crushing under different boundary conditions. Creep occurs as soil deforms over time under a constant loading condition; whereas relaxation is a phenomenon in which stress drop occurs after soil subjected to a constant strain level (Mitchell and Soga 2005). Using a triaxial configuration, researchers found that a higher original deviator stress level or a higher shear strain level will result in a higher stress relaxation of granular sands

(Lade 2007; Lade and Karimpour 2015; Lade et al. 2010). Similar dependencies of granular relaxation on the strain rate and the stress level were also obtained using an oedometer configuration (Brujić et al. 2005; Miksic and Alava 2013) or using numerical simulations (Xu et al. 2018). The stress relaxation mechanism of granular sands was explained using static fatigue, a timedelayed process where failure occurs at a load lower than the value required for short-term failure (Lade and Karimpour 2010; Lade and Karimpour 2015; Michalowski and Nadukuru 2012). At the commencement of relaxation, the soil structure relies on force chains to transmit the applied stress; as time goes by, particle fracture happens because of static fatigue, resulting in particle rearrangement and formation of new force chains. Since the loading boundary does not move, stress reduction occurs. Moreover, for soil relaxation under low confining pressures, soil particle crushes in the form of abrasion; friction at particle-particle contacts and particle rearrangement govern the relaxation behavior. For soil relaxation under high confining pressures, particle crushing and particle rearrangement dominate the relaxation behavior. The relaxation behavior of soils was also observed during soil penetration processes. Atkinson et al. (2019) and Atkinson et al. (2020) found that the penetration resistance is sensitive to the soil relative density but insensitive to stress levels and soil types, while soil relaxation is sensitive to all the three aspects. The results were used to develop a soil classification technique for extraterrestrial exploration by studying the penetration and relaxation behaviors of lunar soils subjected to a constantdisplacement-rate penetration. Yet very few efforts have been made to study whether soil penetration can benefit from soil relaxation.

In this paper, we use a combined technique of photoelasticity and image processing to investigate the penetration and relaxation in granular materials under two penetration scenarios: a continuous penetration and an intermittent penetration. We attempt to address two major questions: (1) can penetration processes can benefit from soil relaxation? and (2) what happens at the particle levels to the granular packings under relaxation?

METHODOLOGY

Experimental Setup. The penetration testing system depicted in (Huang et al. 2020) was used for the tests (See Figure 1(a)). A penetrator is designed and consists of a fixture (purple), a protrusible triangular tip (red), and a hollow rectangular body (yellow and orange), as shown in Figure 1(b). The fixture is used for mounting the penetrator to the testing system. A thin solid rod passes through the hollow rectangular body and connects to the triangular tip. The testing system utilizes a linear actuator (Servocity, HDA12-30, maximum extrusion: 300 mm, static load: 500 lbs) mounted at the center of the top bar to advance the triangular tip downward. The linear actuator is a stepper motor type actuator and controlled by a microcontroller (Arduino Uno). It extrudes the shaft by turning of a leadscrew inside, which prevents any backslash or upward motion of the shaft once the extrusion motion is stopped. A 250 kg load cell is attached to the end of the shaft for measuring the resistive force during the penetration tests. The penetrator is embedded in a thin transparent acrylic chamber, which is filled with 3705 photoelastic particles. These photoelastic particles are obtained via water cutting photoelastic plates (Vishay Precision Group, PSM-1, thickness = 6.35 mm, Elastic modulus = 2.5 GPa, Poisson's ratio = 0.38), and particle diameters are 6mm, 8mm, and 10mm. The chamber is lodged firmly on the testing system and between two polarizer filters, with an LED light source at the back (Figure 1(c)). Two cameras are used for image collection during the tests: one with a polarizer sheet covering the lens focuses on the chamber center to snapshot the force chains; the other is placed right above the former and focuses slightly above the chamber center to snapshot the corresponding configuration of the granular packing. Synchronization of these two cameras is realized through IR remote control. A digital watch is attached to the chamber, so that the polarized images (taken with polarizer filter) and the non-polarized images (taken without polarizer filter) can be matched based on the time displayed on images.

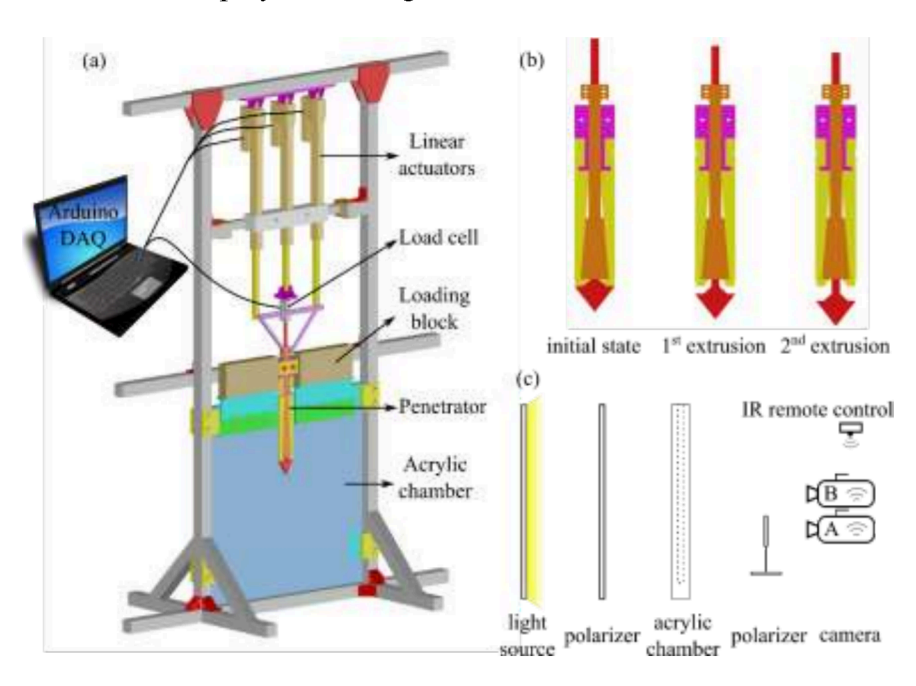


Figure 1. Penetration testing system used for the tests. (a) a general schematic; (b) penetrator; (c) spatial arrangement of the lab testing set up.

Testing Scenarios. As illustrated in Figure 2, two testing scenarios are considered in this study: one is continuous pure penetration (or "CPP"), the other is intermittent pure penetration (or "IPP"). The "IPP" starts with a 16.7s continuous penetration stage (1st penetration stage) and ends with an 8.4s continuous penetration stage (2nd penetration stage); a 1.0 h pausing stage (pausing stage) is involved and separates these two penetration stages. The linear actuator stopped extrusion and holds a constant position during the pausing stage. The "CPP" only involves a 24.3s continuous penetration stage. For both testing scenarios, the tip penetration rate is set as 0.76 mm/s to avoid dynamic penetration effects. In total, three "CPP" tests and four "IPP" tests are conducted.

Testing Procedure. Each penetration test starts with sample preparation, which requires the acrylic chamber and the penetrator to be detached from the system. The chamber is laid flat and the photoelastic particles are randomly and loosely distributed across the entire chamber. Afterward, the penetrator is slowly inserted into the loose granular packing. The chamber is then erected and maintained vertically with the penetrator fixed. The chamber and the penetrator are then secured on the testing system, and a constant vertical confinement is applied to the prepared granular packing. During the tests, the central linear actuator extrudes and pushes the thin rod downward, causing the triangular tip to penetrate the photoelastic granular packing; penetration resistive force and images of the granular packing during the penetration process are collected for analysis. To enhance the test repeatability, a strategy is taken to ensure a relatively consistent initial packing condition among all the samples before the penetration tests. Specifically, the

sample preparations after the first test only involve manually loosening the granular packing to release the residual stresses of particles from previous penetration test, without taking all the particles out of the chamber for re-distributing.

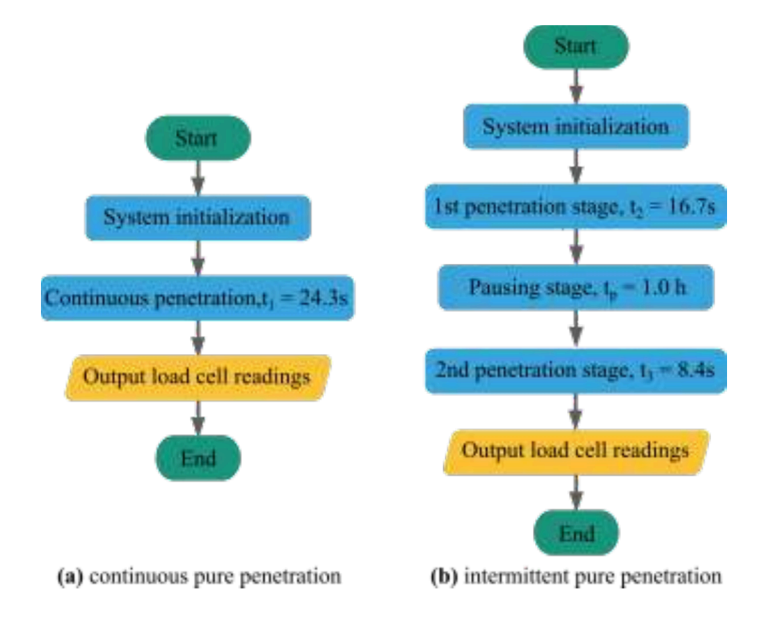


Figure 2. Testing scenarios considered in this study. (a) continuous pure penetration ("CPP"); (b) intermittent pure penetration ("IPP").

Image Processing. The image processing technique developed by Mahabadi and Jang (2017) is implemented in this study to extract information of particle size and location from the non-polarized images. In general, the original non-polarized image is first binarized based on the intensity of the red channel of each pixel. An extended Hoshen-Kopelman algorithm is then used to find all the clusters (here referring to the photoelastic particles) and their belonging pixels(Al-Futaisi and Patzek 2003; Hoshen and Kopelman 1976). The longest distance between two pixels in the same cluster is determined as the diameter of the particles. And the center of the identified diameter becomes the center of the particle. Using this algorithm, the size and position of all the particles are extracted from the non-polarized images. The particle displacement field is then obtained through vectorized subtraction of particle locations of two different moments. It is observed that the thickness of the particle may affect the diameter of particles extracted through this procedure. This happens due to the deviation of the camera angle from the axis perpendicular to the chamber and this effect is pronounced in boundary regions. In order to deal with this problem, all the measured sizes are confirmed to be the same as the actual particle size (1.0 cm, 0.8 cm, and 0.6 cm in diameter).

RESULTS

Resistive Force. Figure 3 shows the penetration curves of both tests. In general, the resistive force of CPP evolves in a way similar to the penetration resistance of common Cone Penetration Tests (Arroyo et al. 2011; Butlanska 2014; Butlanska et al. 2013). It first increases as the triangular tip advances, and then reaches a stable value after 7.4s. The evolution of the resistive force of IPP differs from CPP and depends on the testing stages. Specifically, the resistive force evolves in a pattern similar to that of CPP during the 1st penetration stage, followed by a gradual decrease

during the long pausing stage; afterward, the resistive force increases again and returns to a level comparable to that of CPP by the end of 2nd penetration stage. For both CPP and IPP, deviation of the average resistive force is small at the beginning of the penetration tests, and becomes increasingly obvious as the triangular tip advances to a deeper elevation. This may be attributed to the discrete nature of the granular packing, limited particle-tip contact number, and different initial packing conditions.

Figure 3(b) compares the development of the resistive force during two penetration scenarios. In the 1st penetration stage, the resistive force of IPP has a root mean square (RMS) value (124.51 N) slightly higher than that of CPP (118.75 N), which might be due to a higher average initial packing condition of IPP. Nonetheless, the RMS of the resistive force of IPP (144.82 N) is lower than CPP (161.19 N) in the 2nd penetration stage, which is equivalent to a 10.2% reduction. This difference indicates that separating a continuous penetration with pausing stages facilitate penetration by reducing the penetration resistance. If the resistive forces are normalized so that both IPP and CPP have a same level of resistive force during the 1st penetration stage, the relative reduction of resistive force due to pausing is 13.6%.

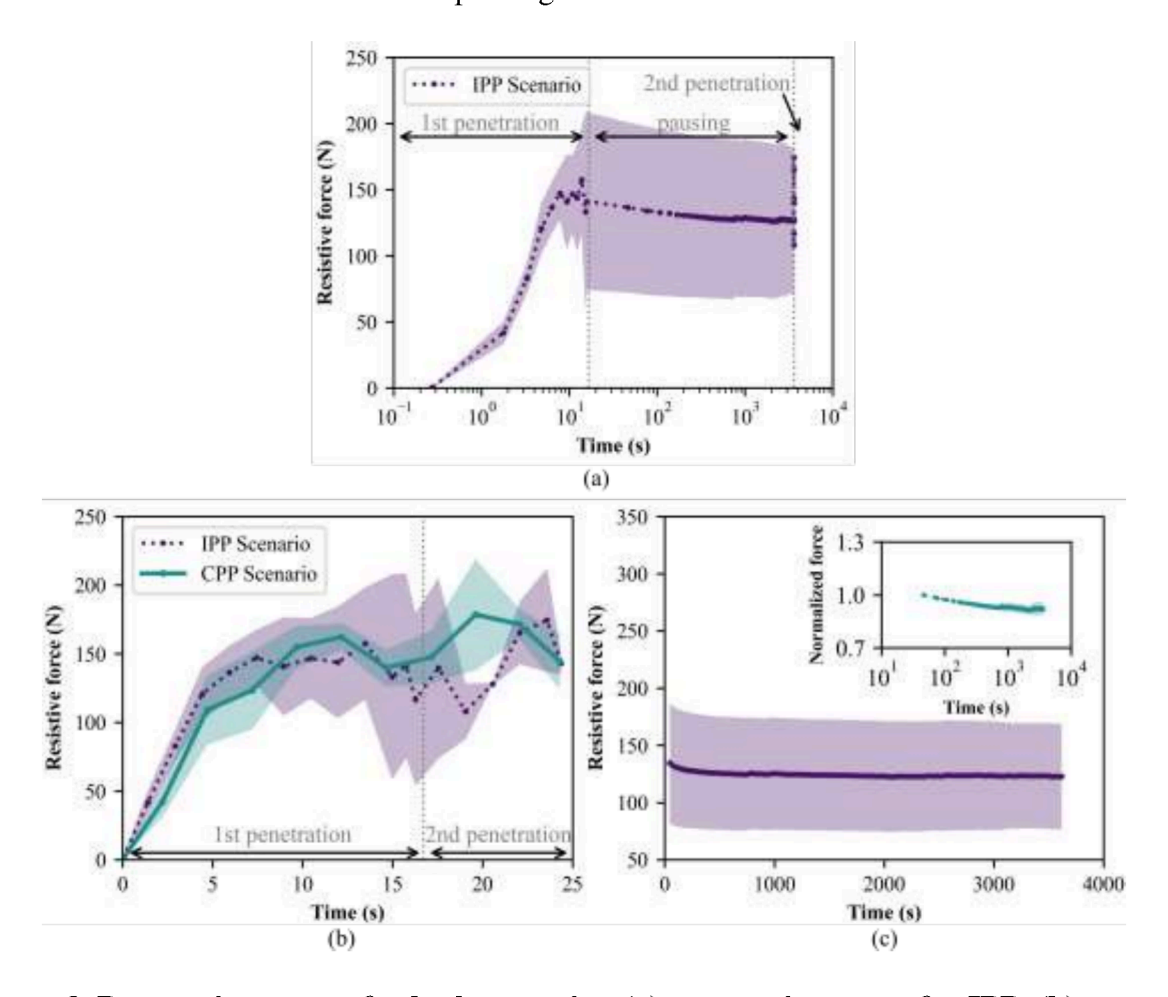


Figure 3. Penetration curves for both scenarios. (a) penetration curve for IPP; (b) penetration curves for both IPP and CPP during the penetration stages; (c) penetration curve for IPP during the pausing stage. The dotted curve indicates the average resistive force, while the shaded area represents the corresponding standard deviation from the average value for each scenario.

The average resistive force decreases relatively fast in the first 150 seconds and only decays gradually afterward (Figure 3(c)). Significant deviations are also observed, which may be due to different initial resistive forces of the four IPP tests at the commencement of the pausing stage. After normalizing the resistive force data of each test by the corresponding initial value, the curves collapse to one with a negligible deviation, implying that the relaxation pattern is independent of the initial penetration resistive force or initial packing of the sample. The normalized resistive force almost linearly decreases with logarithm of time during the long pausing stage.

Load Transfer. Figure 4 presents the evolution of force chains during a selected IPP test. In general, the force chains evolve in a pattern consistent with the evolution of resistive force. Strong force chains form as the triangular tip advances downward at the beginning of the test (from Figure 4 (a) to (b)), and stay at a comparable level since the halfway of 1st penetration stage. These strong force chains originate from the tip with directions perpendicular to the tip surface, and terminate at the external boundaries. Depending on the distributed area, force chains above the triangular tip shoulder tend to incline upward and sideways, whereas force chains below the tip extend downward and sideways.

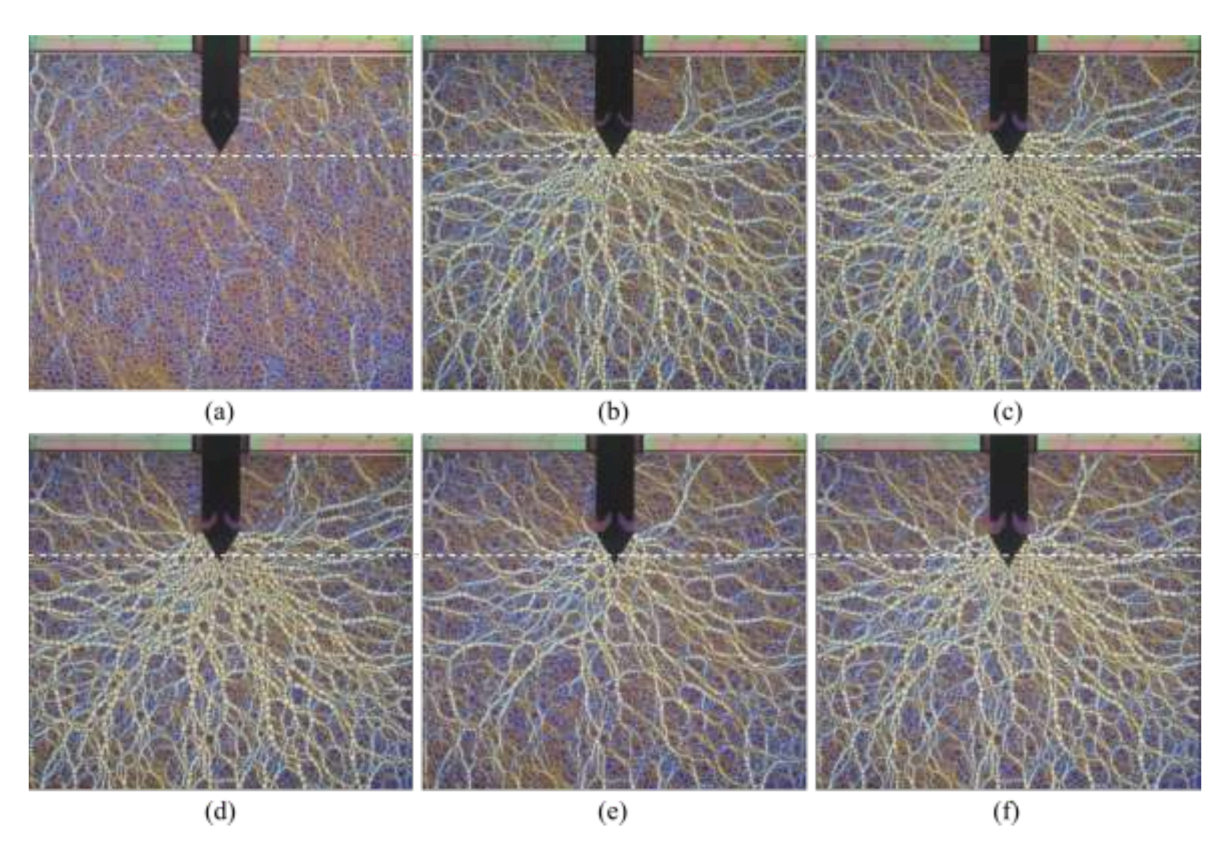


Figure 4. Evolution of force chains during penetration for IPP. (a) Initial state; (b) halfway of 1st penetration stage; (c) end of 1st penetration stage; (d) end of pausing stage; (e) halfway of 2nd penetration stage; (f) end of 2nd penetration stage. The white dotted line indicates the elevation of the triangular tip at different stages relative to the initial stage.

Since the local refractive index of photoelastic material varies with the load applied, such variation causes not only fringe patterns, but also light intensities on a photoelastic particle. In other words, the light intensity indicates the amount of stress applied, while orientation of the

fringe pattern (or light path) on each particle represents the load-transferring direction. Therefore, by conducting pixel-wise light intensity subtractions between polarized images taken at different moments, the relative change of the force chains can be visualized to indicate the range and magnitude of increase (stress development) or decrease (stress relaxation) of the contact forces. Figure 5 presents the stress development and relaxation during the pausing stage obtained by subtracting the green-channel pixel values of Figure 4(c) and Figure 4(d). A factor of 0.8 is applied to the pixel matrix to highlight the difference for an intuitive comparison. It can be concluded that during the pausing stage, both stress development and relaxation occur, although stress relaxation dominates. Significant stress relaxation around the tip mainly occurs in the horizontal direction. Since penetration resistance is affected by lateral confinement (Salgado et al. 1997), it is thus expected that the 2nd penetration after the pausing stage would lead to a lower penetration resistance.

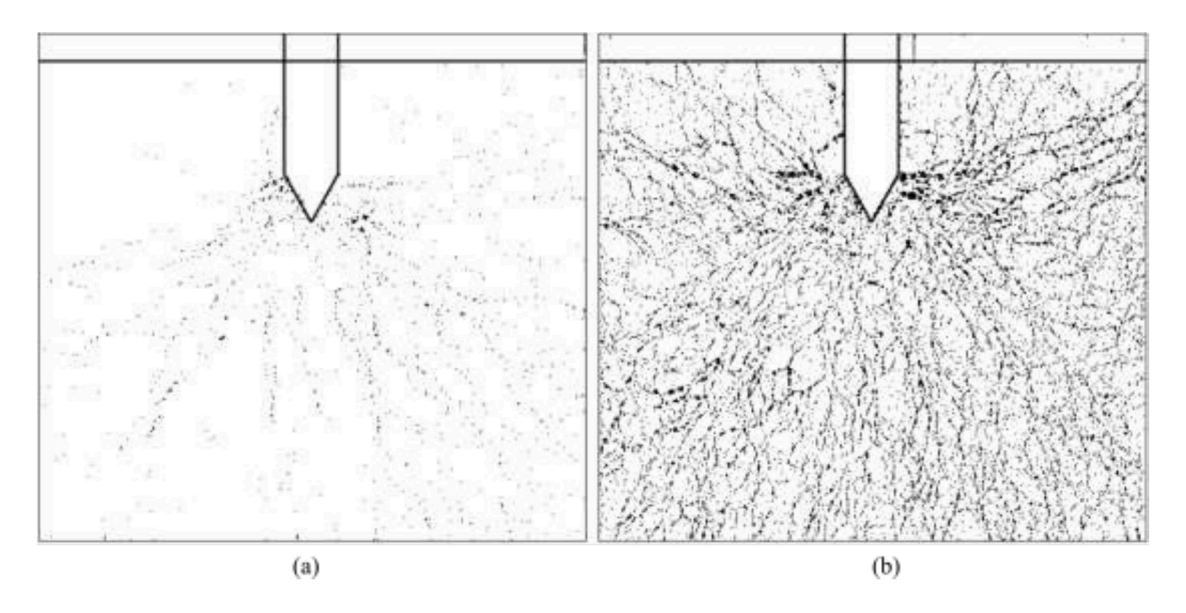


Figure 5. Stress development and relaxation during pausing stage of IPP. (a) stress development; (b) stress relaxation. All the pixel values in the difference pixel matrices are binarized to highlight the areas of stress development and relaxation.

Displacement Field. Figure 6 presents the particle displacement fields in the first 30 min and the last 30 min of the pausing stage for a selected IPP test. The length of the arrow is scaled based on the particle displacement and indicates the travel distance of the particles. It is observed that particles in the granular packing displace randomly and uniformly throughout the pausing stage, with an average travel distance of 0.09 mm in the first 30 min and 0.08 mm in the latter 30 min. The displacement fields confirms that particle rearrangement occurs.

DISCUSSION

In current test configuration, both the stress level and strain rate are low. Particle crushing occurs in the form of abrasion. This is confirmed by the powders remaining near the tip area in the chamber after the tests. Hence, the behavior of the granular packing is governed by the time-dependent friction at the interparticle contacts and the slow particle rearrangement (Lade and Karimpour 2015). The evolution of particle displacement field and average resistive force match

the stress relaxation features of granular sands under conditions of a low initial strain rate and a low stress level (Atkinson et al. 2019; Lade and Karimpour 2015; Miksic and Alava 2013).

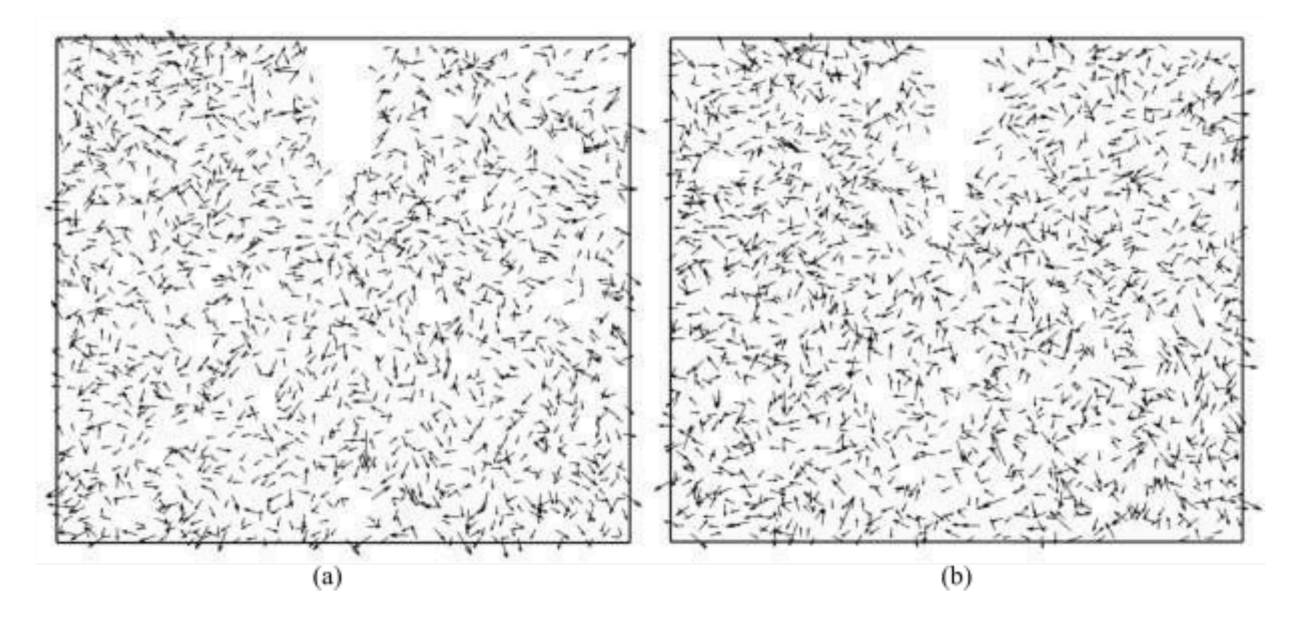


Figure 6. Particle displacement field of the granular packing (a) for the first 30 min and (b) latter 30 min of the pausing stage in IPP. To highlight the evolution of displacement field, only magnitude higher than the average value are presented. The length of all the vectorized arrows is amplified by 3 times for a clearer view.

Pausing or interruption during penetration processes is common in engineering practice. A typical example is adding push rods during cone penetration test (ASTM_D5778-20). It is a common practice to remove data points around the short pausing periods, avoiding the influence of excess pore pressure dissipation on the startup readings of the next push. Findings of this study suggest that soil particles rearrangement also occurs during the pausing stage and results in a lower resistive force at the beginning of the subsequent penetration process. The resulting resistance reduction may depend on the effective stress level, particle shape and penetration rate etc. Further studies on correlations between the pausing-induced resistance reduction and these factors are necessary to provide a reference to similar situations in engineering practice.

Nevertheless, limitations exist. Firstly, the repeatability of the tests can be improved, indicated by the appreciable deviation of resistive force curves in Figure 3. A standard sample preparation method is desired in the future to improve the test repeatability. Secondly, boundary effect exists in current testing configuration. The ratio between chamber width and the penetrator width is 10, which is smaller than the recommended value in previous work (Bolton et al. 1999; Butlanska et al. 2013; Gui and Bolton 1998). A larger chamber test or tests with smaller particles and penetrators can be conducted to evaluate the scaling effects on stress relaxation.

CONCLUSIONS

Using a combined technique of photoelasticity and image processing, it is confirmed that pausing during penetration in a granular sample causes stress relaxation and a subsequent penetration in the relaxed sample results in a lower penetration resistance. The stress relaxes near lin-

early with the logarithm of time. The stress relaxation results in a 10% reduction of penetration resistive force within a limited penetration distance, beyond which the resistive force climbs back to a level comparable to that in a continuous penetration. The particle level contact force and displacement data imply that the significant relaxation mainly occurs around the tip and that it is due to interparticle frictional-sliding and the consequent particle rearrangement.

ACKNOWLEDGEMENT

This material is based on the work primarily supported by the National Science Foundation (NSF) under award number CMMI-1849674. Any opinions, findings and conclusions, or recommendations expressed in this material are those of the authors, and do not necessarily reflect those of the NSF.

REFERENCES

- Al-Futaisi, A., and Patzek, T. W. (2003). "Extension of Hoshen–Kopelman algorithm to non-lattice environments." *Physica A: Statistical Mechanics and its Applications*, 321(3-4), 665-678.
- Arroyo, M., Butlanska, J., Gens, A., Calvetti, F., and Jamiolkowski, M. (2011). "Cone penetration tests in a virtual calibration chamber." *Geotechnique*, 61(6), 525-531.
- ASTM_D5778-20. Standard Test Method for Electronic Friction Cone and Piezocone Penetration Testing of Soils. ASTM International, West Conshohocken, PA, 2020.
- Atkinson, J., Prasad, M., Abbud-Madrid, A., and Dreyer, C. B. (2019). "Penetration and relaxation behavior of dry lunar regolith simulants." *Icarus*, 328, 82-92.
- Atkinson, J., Prasad, M., Abbud-Madrid, A., and Dreyer, C. B. (2020). "Penetration and relaxation behavior of JSC-1A lunar regolith simulant under cryogenic conditions." *Icarus*, 346, 113812.
- Bolton, M. D., Gui, M.-W., Garnier, J., Corte, J. F., Bagge, G., Laue, J., and Renzi, R. (1999). "Centrifuge cone penetration tests in sand." *Géotechnique*, 49(4), 543-552.
- Bowman, E. T., and Soga, K. (2005). "Mechanisms of setup of displacement piles in sand: laboratory creep tests." *Canadian geotechnical journal*, 42(5), 1391-1407.
- Brujić, J., Wang, P., Song, C., Johnson, D. L., Sindt, O., and Makse, H. A. (2005). "Granular dynamics in compaction and stress relaxation." *Physical review letters*, 95(12), 128001.
- Butlanska, J. (2014). Cone penetration test in a virtual calibration chamber.
- Butlanska, J., Arroyo, M., Gens, A., and O'Sullivan, C. (2013). "Multi-scale analysis of cone penetration test (CPT) in a virtual calibration chamber." *Canadian Geotechnical Journal*, 51(1), 51-66.
- Charlie, W. A., Rwebyogo, M. F., and Doehring, D. O. (1992). "Time-dependent cone penetration resistance due to blasting." *Journal of geotechnical engineering*, 118(8), 1200-1215.
- Chow, F., Jardine, R., Nauroy, J., and Brucy, F. (1997). "Time-related increases in the shaft capacities of driven piles in sand." *Geotechnique*, 47(2), 353-361.
- Gui, M., and Bolton, M. (1998). "Geometry and scale effects in CPT and pile design." *Geotechnical site characterization*. Edited by P. K. Robertson and P. W. Mayne. Balkema, Rotterdam, 1063-1068.
- Hoshen, J., and Kopelman, R. (1976). "Percolation and cluster distribution. I. Cluster multiple labeling technique and critical concentration algorithm." *Physical Review B*, 14(8), 3438.

- Huang, S., Mahabadi, N., and Tao, J. "Impact of Shell Opening of a Model Razor Clam on the Evolution of Force Chains in Granular Media." *Proc.*, *Geo-Congress* 2020: *Biogeotechnics*, American Society of Civil Engineers Reston, VA, 272-281.
- Lade, P. V. (2007). "Experimental study and analysis of creep and stress relaxation in granular materials." *Advances in Measurement and Modeling of Soil Behavior*, 1-11.
- Lade, P. V., and Karimpour, H. (2010). "Static fatigue controls particle crushing and time effects in granular materials." *Soils and foundations*, 50(5), 573-583.
- Lade, P. V., and Karimpour, H. (2015). "Stress relaxation behavior in Virginia Beach sand." *Canadian Geotechnical Journal*, 52(7), 813-835.
- Lade, P. V., Nam, J., and Liggio, C. D., Jr. (2010). "Effects of particle crushing in stress drop-relaxation experiments on crushed coral sand." *Journal of Geotechnical and Geoenvironmental Engineering*, 136(3), 500-509.
- Mahabadi, N., and Jang, J. (2017). "The impact of fluid flow on force chains in granular media." *Applied Physics Letters*, 110(4), 041907.
- Michalowski, R. L., and Nadukuru, S. S. (2012). "Static fatigue, time effects, and delayed increase in penetration resistance after dynamic compaction of sands." *Journal of Geotechnical and Geoenvironmental Engineering*, 138(5), 564-574.
- Miksic, A., and Alava, M. J. (2013). "Evolution of grain contacts in a granular sample under creep and stress relaxation." *Physical Review E*, 88(3), 032207.
- Mitchell, J. K., and Soga, K. (2005). *Fundamentals of soil behavior*, John Wiley & Sons New York.
- Salgado, R., Mitchell, J., and Jamiolkowski, M. (1997). "Cavity expansion and penetration resistance in sand." *Journal of Geotechnical and Geoenvironmental Engineering*, 123(4), 344-354.
- Xu, M., Hong, J., and Song, E. (2018). "DEM study on the macro-and micro-responses of granular materials subjected to creep and stress relaxation." *Computers and Geotechnics*, 102, 111-124.